

SUPPLEMENTARY MATERIAL

Bacterial-mediated Selenium Nanoparticles as Highly Selective Antimicrobial Agents with Anticancer Properties

David Medina-Cruz,^a Linh B. Truong,^a Eduardo Sotelo,^b Lidia Martínez,^c María Ujué González,^d Yves Huttel,^c Thomas J. Webster,^e José Miguel García-Martín^d and Jorge L. Cholula-Díaz^{* b}

^a Department of Chemical Engineering, Northeastern University, Boston, MA 02115, USA.

^b School of Engineering and Sciences, Tecnológico de Monterrey, Eugenio Garza Sada 2501, Monterrey 64849, NL, Mexico.

^c Instituto de Ciencia de Materiales de Madrid, ICMM-CSIC, Sor Juana Inés de la Cruz 3, Madrid 28049, Spain.

^d Instituto de Micro y Nanotecnología, IMN-CNM, CSIC (CEI UAM+CSIC), Isaac Newton 8, Tres Cantos 28760, Spain.

^e School of Health Sciences and Biomedical Engineering, Hebei University of Technology, Tianjin 300401, China.

* Correspondence: Jorge L. Cholula-Díaz: jorgeluis.cholula@tec.mx

S.1. Kinetic Analysis

A kinetics analysis was performed over 48 h to quantify the proliferation of bacteria when inoculated with different concentrations of Na_2SeO_3 . The objective was to determine the appropriate concentration to maximize the production of SeNPs. The analysis was performed using a SpectraMax M3 spectrophotometer. Bacteria suspension inoculated with different concentrations of Na_2SeO_3 (1, 2, 3, 5 and 10 mM) were loaded into a 96-well plate and analyzed in the spectrophotometer for 48 h with measurements every 4 min at a wavelength of 600 nm (this wavelength was chosen because, unlike UV wavelengths, 600 nm is not harmful to the culture and is also not usually absorbed by yellowish media as the one used for the experiments). Experiments were done in triplicate, and the average data was converted from units of absorbance to CFU/mL using standardized calibration curves. Absorbance unit data was plotted as depicted in **Figure S1**.

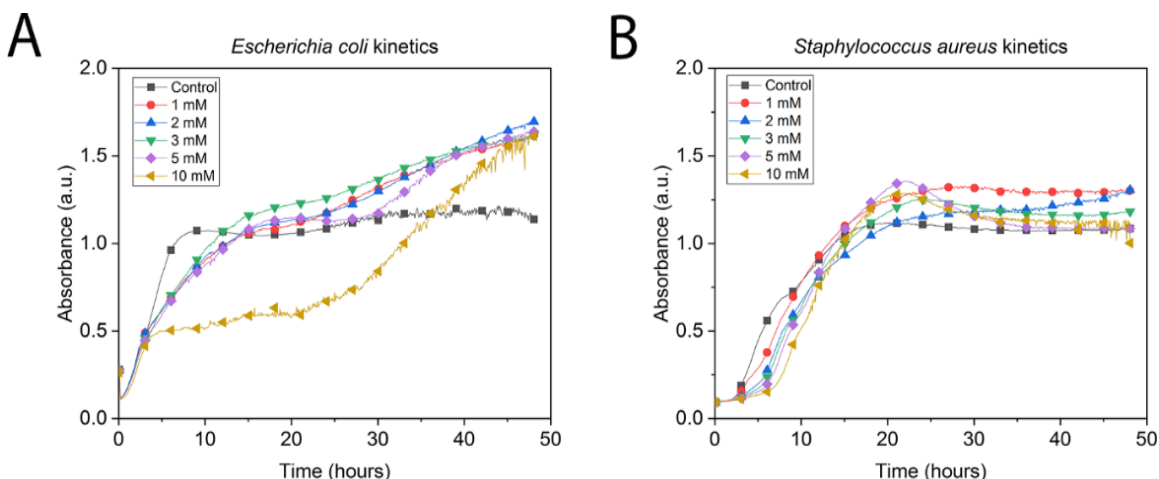


Figure S1. Spectroscopic kinetics analysis (48 h) at a fixed wavelength of 600 nm for both *Escherichia coli* (A) and *Staphylococcus aureus* (B) at different molar concentrations of Na_2SeO_3 . Control is referred to the normal progression of the bacteria with no addition of Se salts. Data = mean, $N = 3$.

As depicted in **Figure S1**, bacterial growth is inhibited by even the smallest concentration of selenium salt (*i.e.*, 1 mM Na_2SeO_3) in the first 10-12 h, after which bacteria start to proliferate like expected from the control curve. The time at which this occurs is called the toleration time (t_T) that is defined as the time at which the bacteria show resistance to SeO_3^{2-} ions. The toleration time of different bacterial cultures inoculated with different concentrations of Na_2SeO_3 (1-4 mM) was plotted in **Figure S2**. Since for EC and MDR-EC bacterial strains the concentration of 2 mM Na_2SeO_3 clearly showed the lowest value for t_T , this concentration was used as the basis of further experiments for the four studies bacterial strains (see main manuscript).

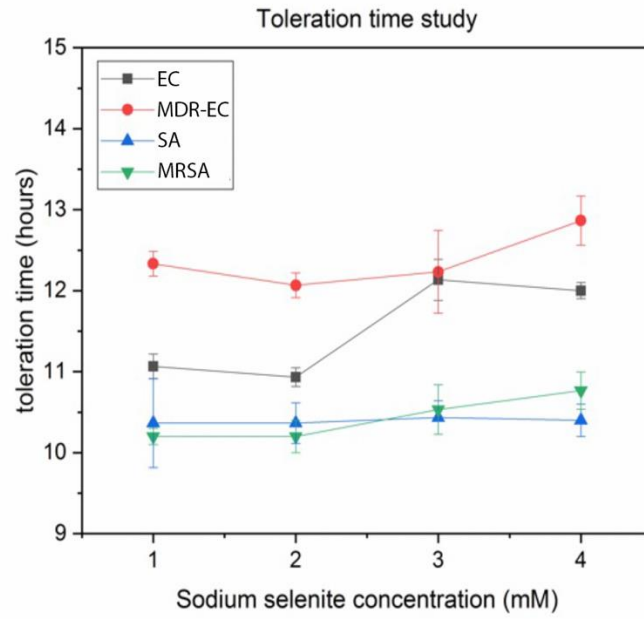


Figure S2. Toleration time (τ_T) study of different bacteria at 1, 2, 3 and 4 mM Na_2SeO_3 concentrations. Data = mean \pm standard error of the mean, $N = 9$.

S.2. Ultraviolet-visible (UV-vis) spectrophotometry analysis

Over the synthesis process, color changes were observed, from a yellowish to a dark orange, in the bacterial media as a consequence of the NPs production (**Figure S3A** and **S3B**). UV-vis spectroscopic characterization was used to follow the synthesis of SeNPs and the changes within the media in terms of NP production. Briefly, several aliquots were taken from the bacterial solution before and after the inoculation with Na_2SeO_3 , following the reaction up to 24 h. Aliquots were transferred to a 96-well plate Falcon clear, and a full absorbance spectrum was recorded from 200 to 800 nm with 20 nm spacing. A 2 mM Na_2SeO_3 concentration was employed for the inoculation (as it gave the best fit for the bacterial proliferation). Experiments were repeated three times, and the average of the measurements was calculated and plotted in **Figure S3**.

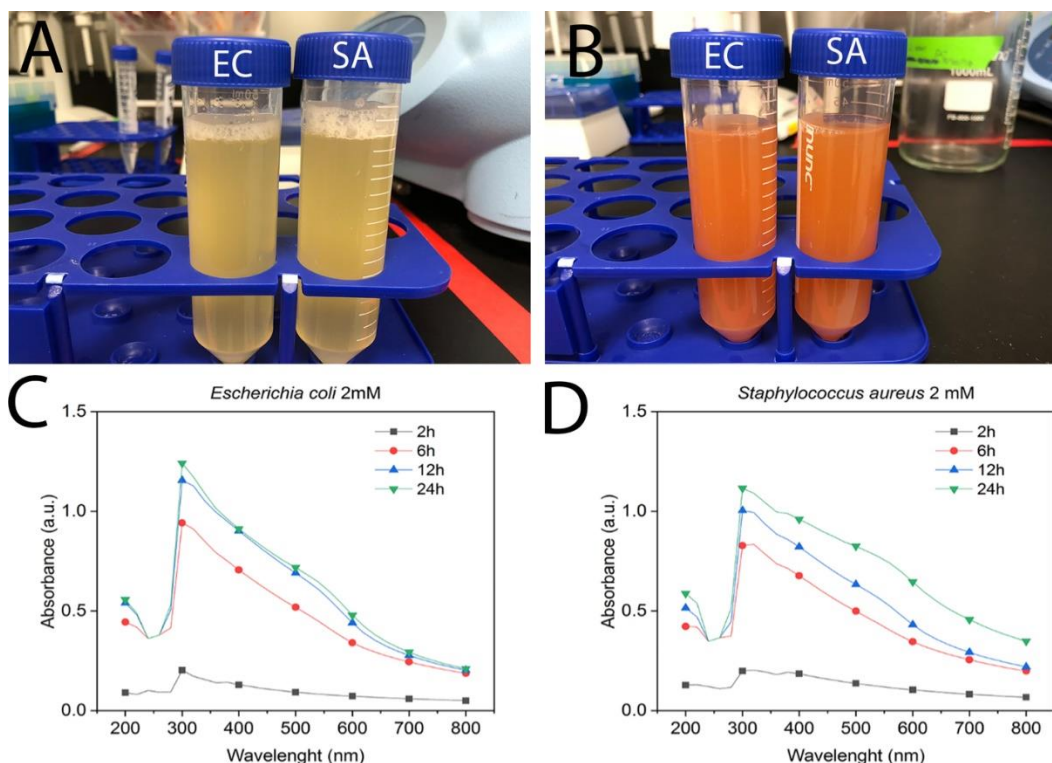


Figure S3. Visual coloration change observed during SeNPs synthesis by *Escherichia coli* (EC) (left tube) and *Staphylococcus aureus* (SA) (right tube) at 0 h (A) and 24 h (B) in the process after addition of selenium salt precursor. MDR-EC and MRSA samples are not shown, but they went through the same behavior in coloration change as the samples presented in the current image. UV-vis spectroscopic analysis for the synthesis of SeNPs using both EC (C) and SA (D) and a 2 mM Na_2SeO_3 solution. Data = mean, $N = 3$.

The UV-vis spectroscopic analysis was able to show the progression of the reaction at different times. Media and bacterial culture absorbance values were subtracted only to show the contribution of Se to the reaction development. As can be seen for EC (**Figure S3C**), there is an intense and wide band at ~ 300 nm, while for SA (**Figure S3D**), the band becomes broader at the same wavelength. The wide broadness of the bands in **Figures S3C** and **S3D** may indicate that nanoparticles of different sizes are being produced. Despite these observed differences, both absorption bands in the UV-vis range are related to the formation of SeNPs³, which is concordant with that reported previously^{4,5}. The height of the absorption band for SeNPs increased significantly (around 4 times) from 2 to 6 h, with a slight further

increase for a time up to 24 h. These results, which were evident for both bacterial strains, revealed that the SeNPs production started shortly after the inoculation and prolonged up to one day of the experiment.

S.3. Reactive Oxygen Species analysis of the synthesis process

For the ROS quantification, 2',7'-dichlorodihydrofluorescein diacetate (H2DCFDA) was used. Briefly, bacterial cells were seeded in a 96 well-plate at a concentration of 10^6 CFU/mL in LB media and the presence of different concentrations of Na_2SeO_3 as well as in control without any salt. The cells were then cultured under standard bacterial culture conditions for up to 48 h. The growth media were then removed, and PBS was added, reaching a final and fixed concentration of $10 \mu\text{M}$. The cells were incubated for an additional 30 min. Subsequently, fresh media was added after buffer removal. Besides, positive controls containing hydrogen peroxide (H_2O_2) at a fixed concentration of $50 \mu\text{M}$ were set in the plates. The intensity of fluorescence was measured at 530 nm while the sample was excited at 485 nm. These wavelengths were indicated by the commercial kit as the most suitable to exert the best quality in fluorescence measurements.

The inhibition of bacterial proliferation observed in **Figure S1** can be explained by oxidative stress, understood as the imbalance between free radicals (oxygen-containing molecules with an uneven number of electrons) and antioxidants inside the cell⁶. A decade ago, the discussion started around the potential involvement of intracellular thiols in SeO_3^{2-} reduction in some bacterial species⁷. For instance, in EC, the SeO_3^{2-} reduction occurs through a pathway involving glutathione (GSH) and different organoselenium intermediates⁸, which is often related to the release of O_2 and creation of oxidative stress, which may lead to a natural delay in the bacteria's growth. However, this hypothesis could not yet be applied to SA, as no data has been reported in the literature.

As shown in **Figure S4**, the addition of 2 mM of Na_2SeO_3 led to an overproduction of ROS at 6 and 12 h. However, at 24 h, enough time after the toleration time (t_τ , see Figure S2) for both bacterial species, the ROS levels went close to the control again. These results may indicate that the bacteria can cope with the ROS increase due to the addition of salts, restoring the levels to normal once the toleration time has been overcome. Therefore, it is possible to hypothesize that the production of SeNPs is a direct consequence of the survival of the bacteria, as they can cope with an increase of ROS, whose concentration will undoubtedly lead to cell death.

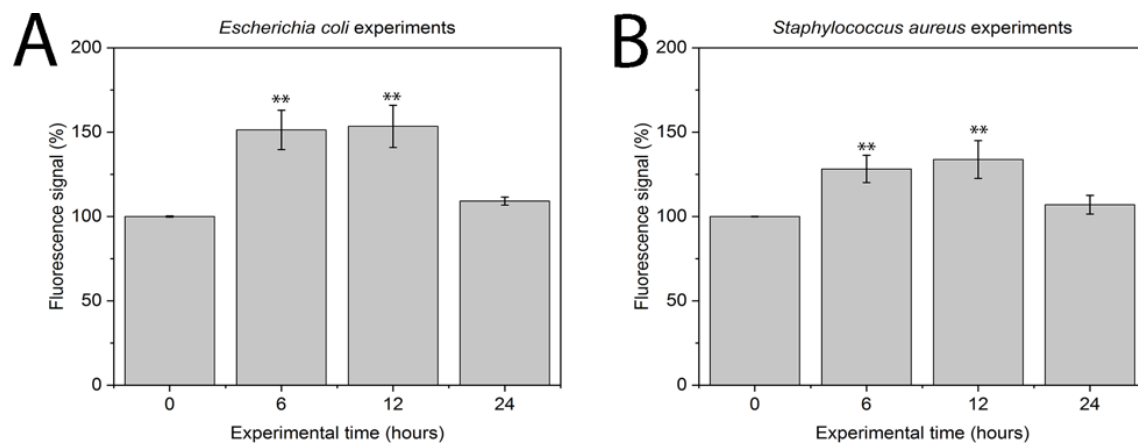


Figure S4. ROS production of *Escherichia coli* (A) and *Staphylococcus aureus* (B) upon addition of 2 mM Na₂SeO₃ at different experimental times. Data = mean +/- standard error of the mean, N = 3. Statistical differences represented by **p < 0.01 versus control.

S.4. Scanning Electron Microscopy (SEM) analysis of non-purified samples

The samples here analyzed were kept in the dispersion in the presence of bacteria and biomolecules coming from them (i.e., without purification process) and were imaged about 3 months after their preparation. SEM characterization was carried out using an FEI Verios 460 scanning electron microscope. Two modes of SEM imaging were used: 1) backscatter electron (BSE) imaging to detect differences in atomic number on and below the surface of the sample; and 2) secondary electron (SE) imaging that collected secondary electrons generated from the constituent atoms excited by inelastic scattering of the incident electrons in the samples to detect sample morphology. For SEM observation, 7 μL of each sample was deposited on clean Si substrates and allowed to dry for more than 24 h. The microscope conditions employed were 2 kV acceleration voltage and 13 pA electron beam current.

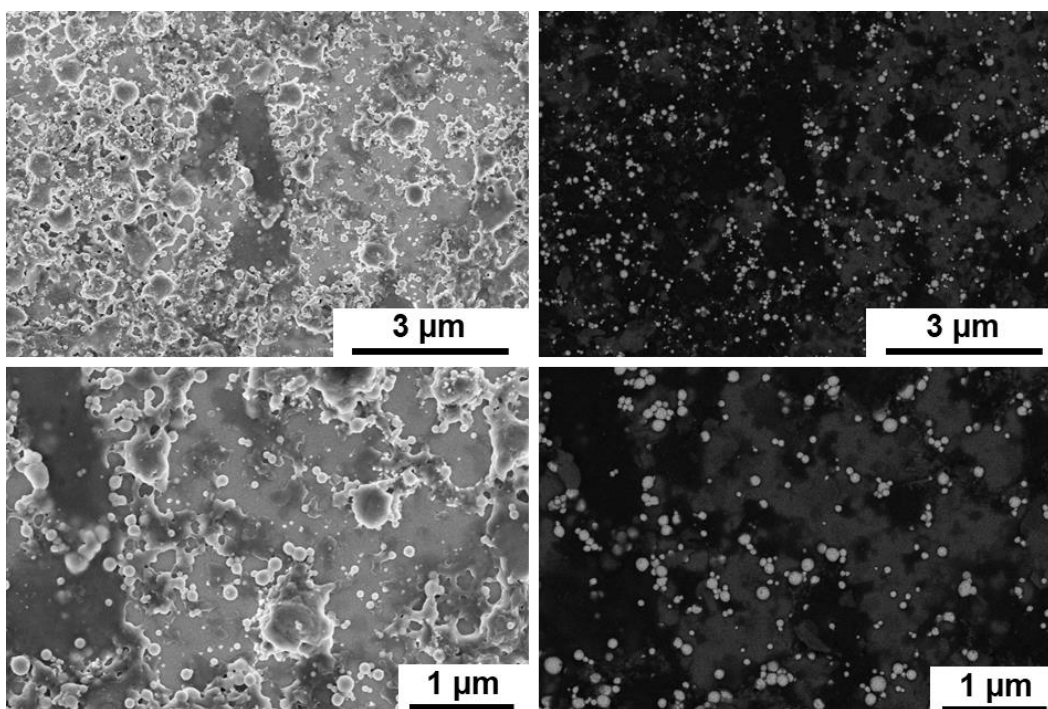


Figure S5. SEM characterization of EC-SeNPs at different magnifications and imaging modes (simultaneous acquisition of secondary and back-scattered electrons for the images in the left and right columns, respectively).

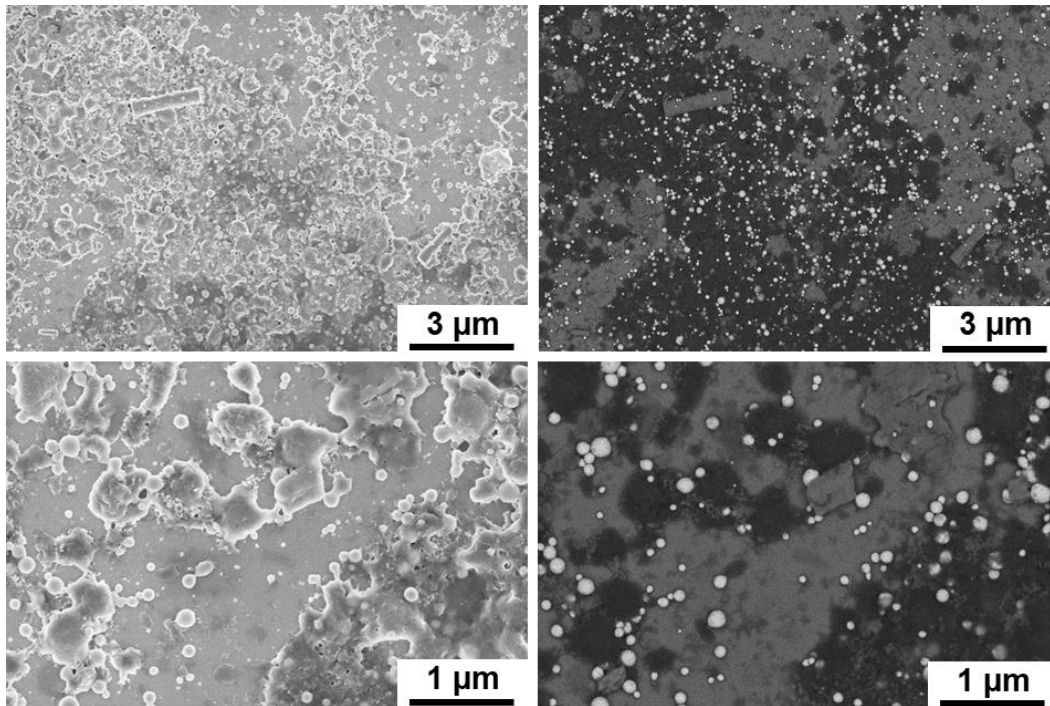


Figure S6. SEM characterization of MDR-EC-SeNPs at different magnifications and imaging modes (simultaneous acquisition of secondary and back-scattered electrons for the images in the left and right columns, respectively).

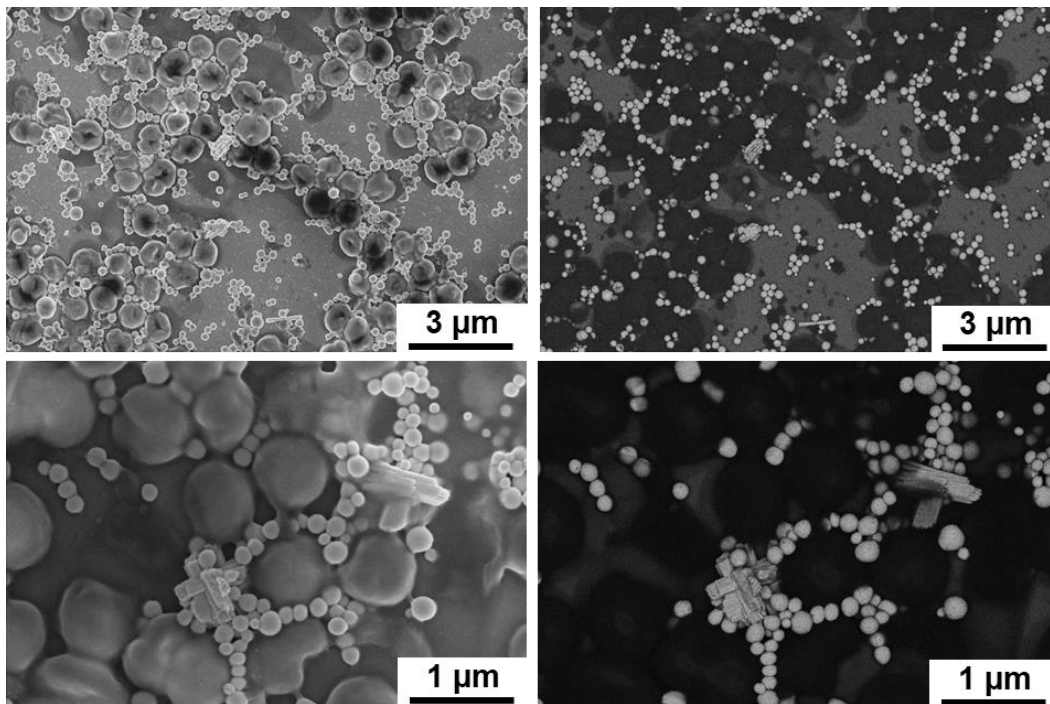


Figure S7. SEM characterization of SA-SeNPs at different magnifications and imaging modes (simultaneous acquisition of secondary and back-scattered electrons for the images in the left and right columns, respectively).

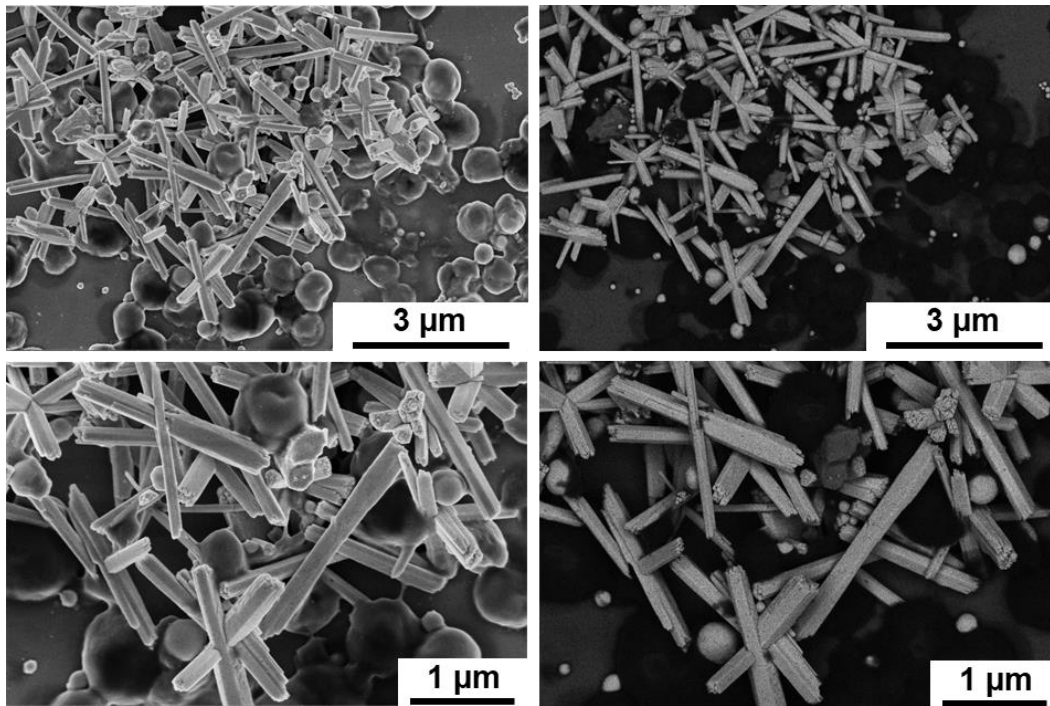


Figure S8. SEM characterization of MRSA-SeNPs at different magnifications and imaging modes (simultaneous acquisition of secondary and back-scattered electrons for the images in the left and right columns, respectively).

SEM images show that, in all cases, the bacteria have produced SeNPs. Compared to the purified samples characterized in Section 3.2 of the main manuscript, there is no significant difference for EC-SeNPs (**Figure S5**) and MDR-EC-SeNPs (**Figure S6**): both exhibit spherical SeNPs with and without purification. However, there is a big difference in the case of the NPs produced by SA and especially MRSA, with and without purification. Spherical morphologies were found for non-purified SA-SeNPs (**Figure S7**), with some small clusters of rod-shaped structures. The concentration of clusters was significantly higher for non-purified MRSA-SeNPs (**Figure S8**), with large rods and only a small proportion of spheres.

It becomes essential to bring to attention that the biomolecules-based coating enclosing the nanostructures and organic debris made it challenging to observe nanoparticles falling in a smaller size range while imaging with secondary electrons. However, in back-scattered electrons mode, nanostructures made of Se ($Z = 34$) were easily distinguished from those features that were part of the organic phase ($Z = 6$ and 8 for C and O, respectively) due to increased signal that depends on the atomic number Z .

S.5. Energy-dispersive X-ray (EDX) Spectroscopy

Energy-dispersive X-ray (EDX) spectroscopy was performed using the same FEI Verios 460 Field-emission scanning electron microscope where SEM imaging was done, with the same non-purified samples. The SEM conditions for the EDX measurements were a 10 kV acceleration voltage and a 400 pA electron beam current. The EDX spectra confirmed that the NPs are made of Se. In the sample, we can also find C, N, O, Na, S, and P (and sometimes Ca and Cl) originating from the cells. For comparison, measurements were acquired with the spot fixed on top of the NPs and out of them, on top of bacteria or organic remnants; in all cases, the NPs showed a substantial content of Se.

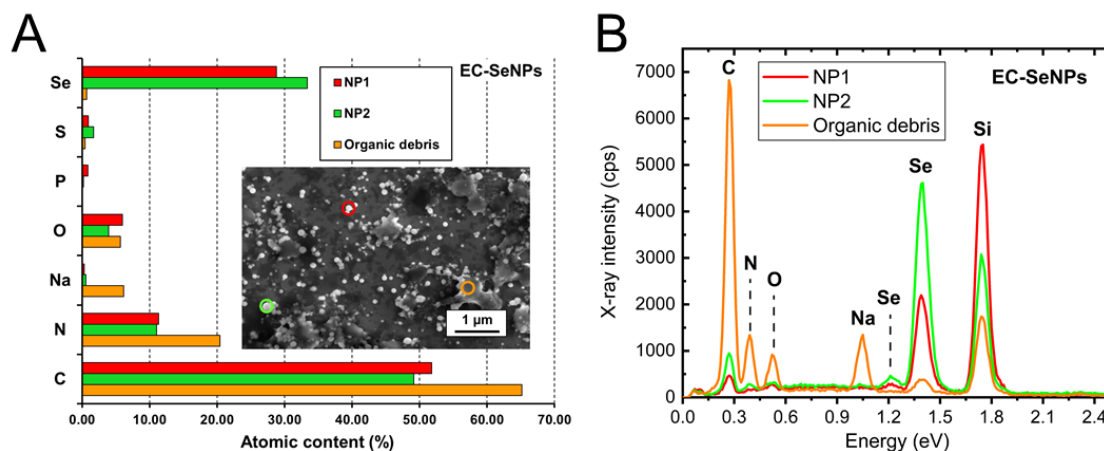


Figure S9. EDX characterization of EC-SeNPs at different spots (A) and the X-ray intensity of the elements (B).

For the EC-SeNPs (**Figure S9**), measurements were done on top of the spherical NPs (NP1 and NP2) and confirmed presence of Se. Here, a large amount of C/N/O was also observed, but it can be attributed to the signal coming from both the NPs organic coating and the debris present in the surroundings. Measurements on top of the organic debris confirmed that Se was concentrated in the NPs.

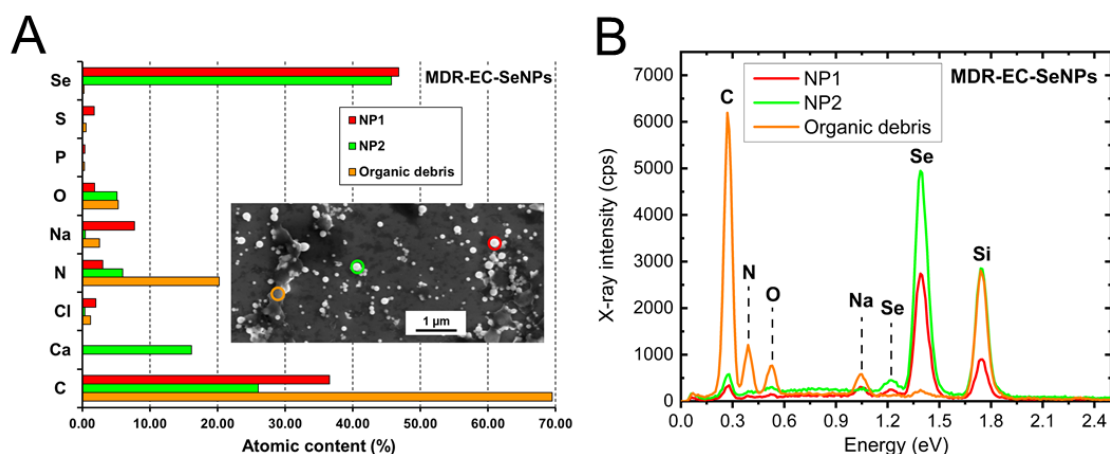


Figure S10. EDX characterization of MDR-EC-SeNPs at different spots (A) and the X-ray intensity of the elements (B).

The MDR-EC-SeNPs sample (**Figure S10**) showed the same behavior. On top of the spherical NPs (NP1 and NP2), there was a detection of a strong content of Se, together with C/O/N elements, which could be associated with the organic coating and the NP surroundings. Almost no Se was detected when the electron beam was placed on top of the organic debris, confirming the absence of Se in the organic matter.

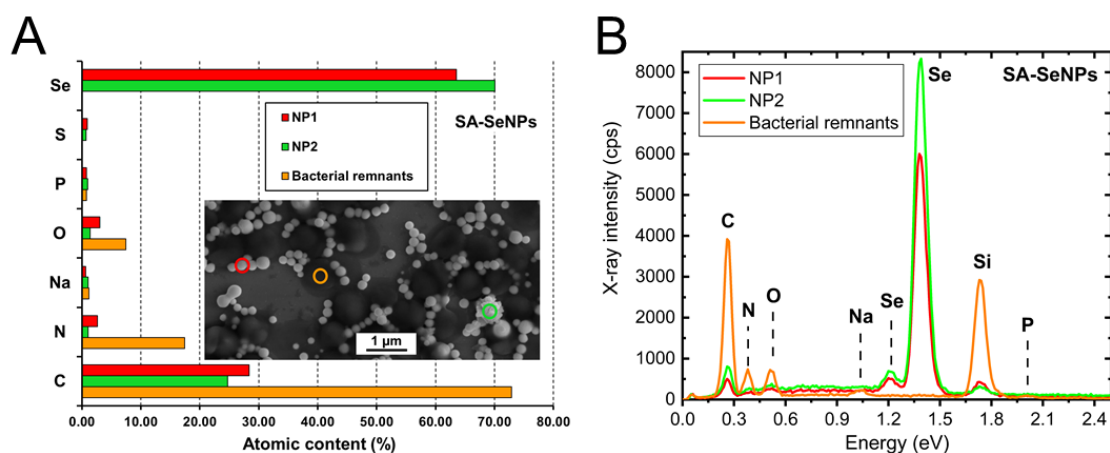


Figure S11. EDX characterization of SA-SeNPs at different spots (A) and the X-ray intensity of the elements (B).

For SA-SeNPs (**Figure S11**), the top of a spherical NP was first checked (NP1), as well as the top of a cluster of small rods presented in the sample (NP2). Both NPs contained a high amount of Se, and no significant differences were seen with EDX. The C content could come from the NP and the surrounding area or some possible organic coating. The rest of the elements were found in low concentrations. The measurement on the top of a SA bacterium remnant showed no presence of Se, and a large concentration of C, N, and O, as expected.

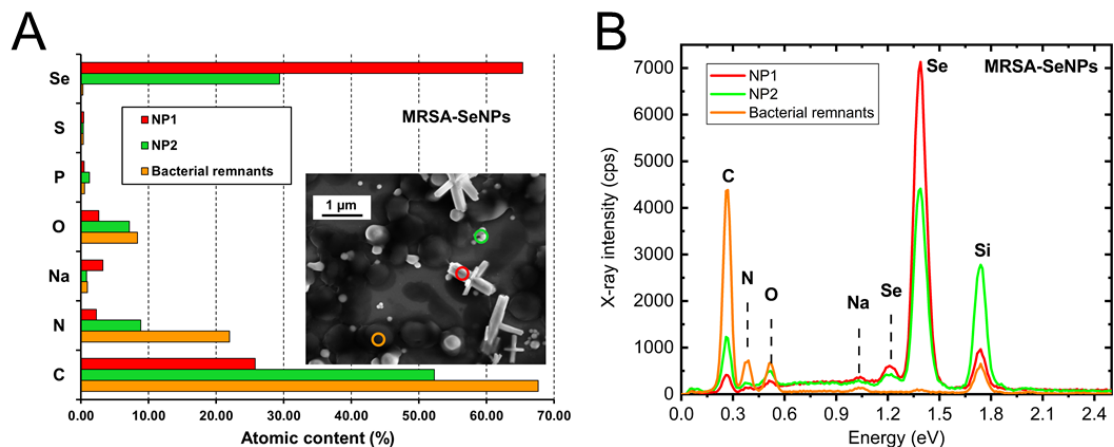


Figure S12. EDX characterization of MRSA-SeNPs at different spots (A) and the X-ray intensity of the elements (B).

In the case of MRSA-SeNPs (**Figure S12**), where most NPs were shaped like rods, the top on a rod-like NP was checked (NP1), as well as the top of a small spherical NP (NP2). In both cases, the content of Se was reasonably high. The presence of more C, N and O in NP2 in comparison to NP1 was likely to be associated with the signal coming from the organic debris observed close to the spherical NPs, as its size was relatively small (and the EDX resolution for the beam energy used is estimated to be around 300 nm). Again, the measurement on the top of a SA bacterial remnant showed no Se presence and a large concentration of C, N, and O, as expected.

S.6. X-ray photoemission spectroscopy (XPS)

Samples of the four different non-purified SeNPs were deposited on Cu substrates and introduced into an Ultra High Vacuum system for their X-ray photoemission spectroscopy (XPS) characterization. The samples were loaded in a vacuum load-lock chamber and then transferred into the analysis chamber with a base pressure of around 10^{-10} mbar. A hemispherical electron energy analyzer (SPECS Phoibos 100 spectrometer) and an Al- K_{α} (1486.29 eV) X-ray source were used for the measurements. Furthermore, the angle between the hemispherical analyzer and the plane of the sample was 60° . For the measurement, an energy step of 0.5 eV and a pass-energy of 40 eV were used to obtain broad scan spectra, while specific core levels spectra (O 1s, N 1s, C 1s, and Se 3d) were measured using an energy step of 0.1 eV and a pass-energy of 20 eV. The spectra were analyzed using the CasaXPS software. Moreover, the absolute binding energies (BE) were quantified by a reference to the C 1s core level peak at 285 eV, measured slightly out of the samples' center to check the adventitious carbon. The contributions from the Al K_{α} satellite lines were subtracted.

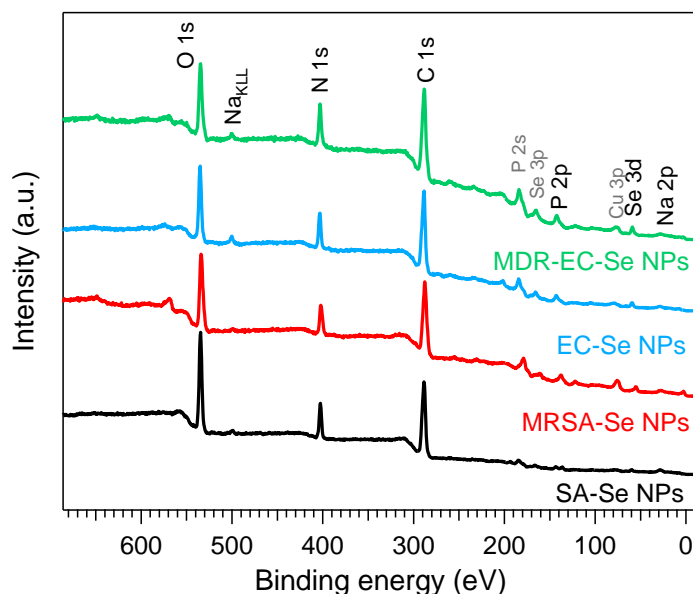


Figure S13. Wide energy range scans of the SeNPs samples. The offset in the intensity is for easier comparison.

Figure S13 presents a wide energy range scan spectra of the samples normalized to the intensity of the O 1s. The samples presented C, O, N, Na, P, Se and possibly small amounts of S. The coincidence in the BE of the primary Se and S peaks makes it difficult to unequivocally assign part of them to S (Note: $BE_{S\ 2p} = 164$ eV). All the samples presented similar compositions. The main difference among them relies on the smaller amount of P and Se in the SA-SeNPs sample. **Table S1** provides the composition of the samples extracted from the analysis of the spectra.

Table S1. Composition of the samples (%_{at}) from the wide energy range scans.

| | Composition % _{at} | | | | | | |
|--------------|-----------------------------|------|-----|------|-----|-----|-----|
| | C | N | Na | O | P | S | Se |
| SA-SeNPs | 58.6 | 11.6 | 2.5 | 25.7 | 0.8 | 0.5 | 0.3 |
| MRSA-SeNPs | 58.6 | 11.3 | 1.9 | 22.3 | 4.8 | 0.0 | 1.1 |
| EC-SeNPs | 61.7 | 12.4 | 1.6 | 19.2 | 4.2 | 0.0 | 0.9 |
| MDR-EC-SeNPs | 63.4 | 11.9 | 1.1 | 17.5 | 4.7 | 0.0 | 1.4 |

The Se 3d core level peaks (**Figure S14**) evidenced three different oxidation states in the samples. The BE of the component described in the following corresponds to the Se 3d_{5/2} (spin-orbit splitting between Se 3d_{5/2} and Se 3d_{3/2} is 0.86 eV): The component at the lowest BE of 55.9 ± 0.1 eV corresponds to elemental selenium⁹; the component at 59.1 ± 0.1 eV can be related to the presence of Se in the form of Na₂SeO₃⁹ And, finally, a third component was observed in the SA-SeNPs sample at a BE of 60.1 eV, an energy intermediate between Na₂SeO₃ (59.1 eV) and Na₂SeO₄ (61.6 eV). Therefore, all the Se in this sample probably presents a mixture of sodium selenite and sodium selenate. The sample MRSA-SeNPs presents the largest proportion of Se⁰ (88% of Se⁰ and 12% of Na₂SeO₃). The sample EC-SeNPs only presents Se in the form of Na₂SeO₃. Finally, the MDR-EC-SeNPs presents 91% of Se in the form of Na₂SeO₃ and the rest in the form of Se⁰. Therefore, depending on the bacterial strains used, differences can be found in the Se oxidation state.

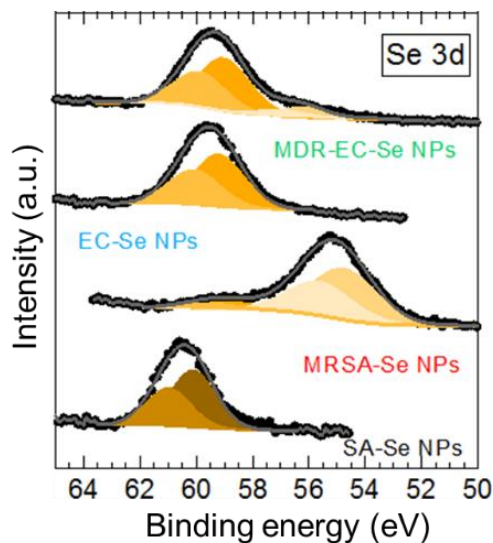


Figure S14. Se 3d core-level spectra of the samples.

Figure S15 presents the C 1s, O 1s, and N 1s core-level peaks of the samples, with a detailed peak analysis in **Table S2**. In the case of the C 1s, the peaks have been fitted using five components typical from organic compounds¹⁰, keeping constant the full width at half maximum (FWHM): C-C/C-H bonds at 285 ± 0.2 eV; C-O / C-N bonds at 286.3

± 0.2 eV; C=O bonds at 288.1 ± 0.2 eV, O-C=O or N-C=O bonds at 289 ± 0.2 eV and the fifth component at 291.0 ± 0.2 eV may be described to the O-(C=O)-O groups.

It can be observed that, depending on the bacteria employed, the proportion of the C 1s components varies. The main difference is observed in the MRSA-SeNPs sample, where a larger proportion of C-C / C-H and C-O / C-N components are present compared to the other samples. This sample presented a smaller proportion of oxidized Se (Figure S14). Apart from this, the SA-SeNPs sample presents the largest carbon proportion in form of O-C=O and O-(C=O)-O. This sample also presented the largest proportion of oxygen and had Se in a higher oxidation state.

The analysis of the O 1s core-level peak evidenced specific differences among the samples. There are two components that are predominant in the O 1s core level peak. According to Clark, these two components correspond to the ester (535.3 ± 0.2 eV) and carbonyl oxygens from the O-(C=O)-O groups, separated by 1.5 eV to lower BE et al.¹¹. Besides, there is a third component at 531 eV that can be ascribed to the presence of C-O bonds or/and O=C-N bonds¹² or NO₂ groups⁹. In the SA-SeNPs, the first two components dominate the spectra. The EC-SeNPs and MDR-EC-SeNPs samples present similar spectra with an increasing proportion of the component at 531 eV. Finally, the MRSA-SeNPs present the same components as the other samples but with a significant increase in carbonyl groups. This result follows the analysis of the C 1s core level, whereas the C=O dominated the C 1s spectra.

Finally, the analysis of the N 1s core level peak reveals the presence of three different components. The main component appeared at a BE of 403.2 ± 0.2 eV. This energy range could be ascribed to different organic compounds, such as (CH₃)₃NO or -(CH₃COO)₄(NO₂)₂⁹. In the case of the MRSA-SeNPs sample, this component appeared at 402.2 eV, closer to the BE of the -N(CH₃)₃ groups.

At a lower BE, there is a component at 400.2 ± 0.2 eV that corresponds to the presence of N-C=O groups. This component is nearly three times more abundant in the MRSA-SeNPs sample than in the others, revealing the different nature of this sample in all its elements. In this sample, the main component is shifted 1 eV in comparison to the other samples. The third component at 405.2 ± 0.2 eV represents less than 10% of the Nitrogen in the samples (not present in the MRSA-SeNPs sample) and could be related to other NO₂ groups.

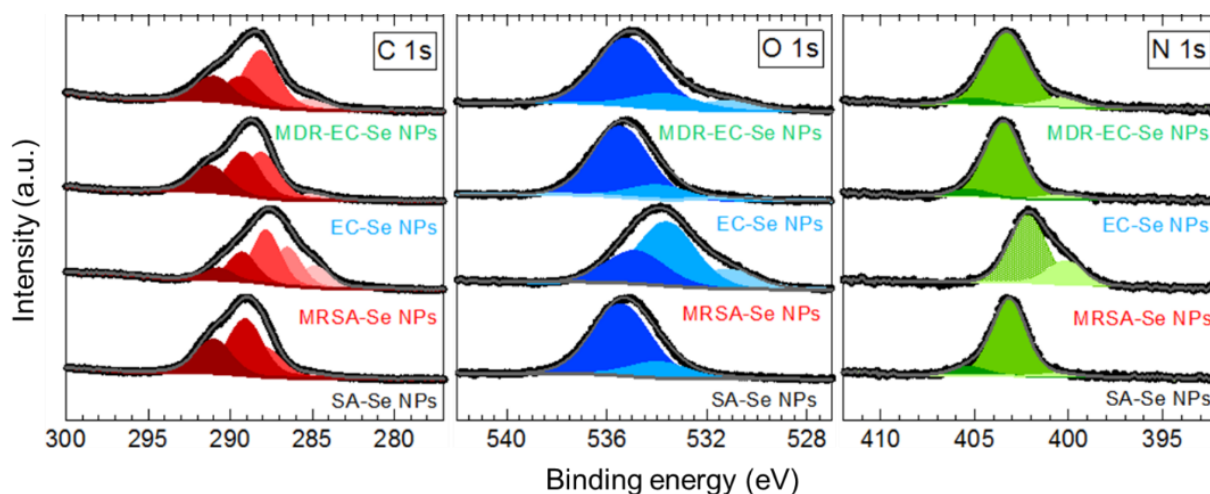


Figure S15. C 1s (left), O 1s (center), and N 1s (right) core level spectra of the samples.

Table S2. Percentage of the components used to fit the C 1s, O 1s, and N 1s core levels.

| | C 1s | | | | | O 1s | | | N 1s | | |
|---------------------|------------|------------|------|----------------|-----------|------|------|------|-------|---|-----------------|
| | C-C C-H | C-O C-N | C=O | O-C=O N-C=O | O-(C=O)-O | C-O | =O | -O- | N-C=O | -NO -(NO ₂) ₂ N(CH ₃) ₃ | NO ₂ |
| SA-SeNPs | 2.2 | 0.0 | 25.2 | 47.2 | 25.4 | 0.9 | 81.3 | 17.8 | 6.6 | 84.5 | 8.9 |
| MRSA-SeNPs | 13.1 | 25.4 | 35.2 | 19.2 | 7.1 | 6.7 | 27.9 | 65.4 | 38.6 | 61.4 | 0.0 |
| EC-SeNPs | 4.4 | 0.0 | 38.5 | 37.1 | 20.0 | 1.2 | 82.4 | 16.4 | 10.0 | 83.0 | 7.0 |
| MDR-EC-SeNPs | 8.4 | 3.1 | 47.7 | 22.5 | 18.3 | 4.1 | 78.7 | 17.2 | 17.1 | 76.1 | 6.8 |

S.7. X-ray diffraction (XRD)

XRD analysis (**Figure S16**) was done to provide useful information about the crystallographic phases within the structures and help correlate microscopic observations. Non-purified samples were used.

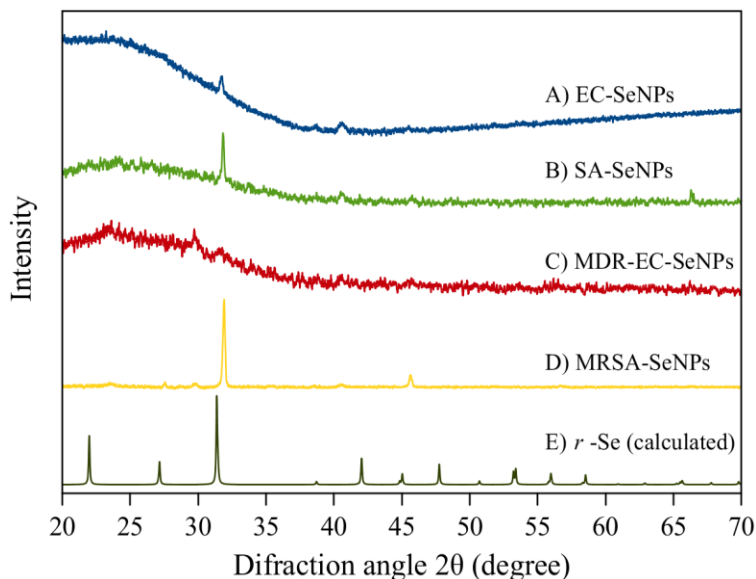


Figure S16. Comparison between the XRD patterns for A) EC-, B) SA-, C) MDR-EC-, D) MRSA-SeNPs, and the calculated rhombohedral Se (*r*-Se). The calculated data were taken from [13].

XRD patterns for EC-, SA-, MDR-EC-, and MRSA-SeNPs are shown in **Figure S16**. A very intense diffraction peak in the diffraction pattern for MRSA-SeNPs was localized at 31° in 2Θ that may be indexed to the crystallographic plane with Miller indices (121) of the rhombohedral Se structure (*r*-Se, space group $R\bar{3}$)¹³, despite its shift to higher 2Θ values. The XRD analysis indicated the lack of lower intensity peaks related to *r*-Se, probably due to the very low signal-to-noise ratio of the samples. In the case of the XRD analysis of EC-SeNPs, SA-SeNPs, and MDR-EC-SeNPs, the diffraction patterns indicate a more abundant amorphous phase than in sample MRSA-SeNPs. However, in the samples EC-SeNPs and SA-SeNPs, it can be noted that the most intense peak is located at a diffraction angle 2Θ around 31° , which is closely related to *r*-Se¹³.

S.8. Stability Analysis

Transmission electron microscopy (TEM) imaging was performed on purified samples after 120 days of synthesis of two samples (SA- and EC-SeNPs) to determine the aqueous solution's stability. A Z-potential was measured for each sample after synthesis and after 120 days.

In general, it was evident that the samples kept their original morphologies and features. For instance, the 120-days old SA-SeNPs (**Figure S17A**) sample showed nanoparticles that remained isolated in solution, together with some isolate aggregation cases with small nanospheres agglomerated with bigger ones. A similar result was observed for EC-SeNPs (**Figure S17B**) that remained isolated in solution. These features are following the freshly synthesized nanomaterials, as can be seen in Fig. 2 (main manuscript).

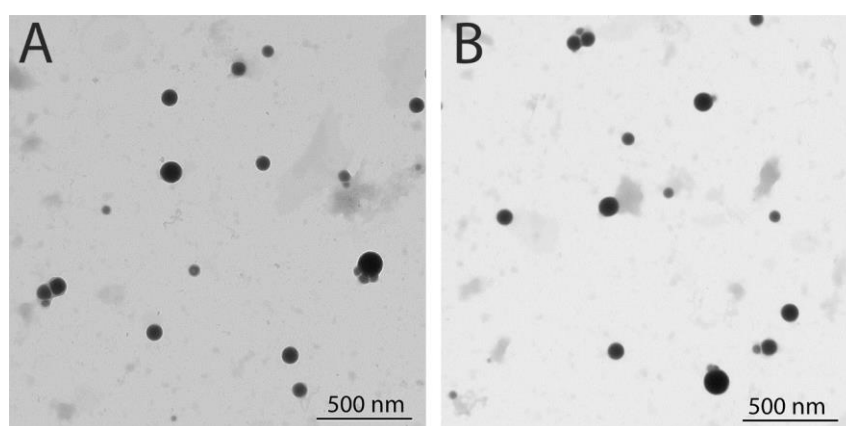


Figure S17. TEM characterization of SeNPs synthesized by SA (A) and EC (B) with 2 mM Na_2SeO_3 solution after 120 days.

The stability analysis through the measurement of the Z-potential of the freshly synthesized and 60-days old Se-based nanomaterials was also carried out. In general, a colloid or suspension is considered stable if the Z-potential is above a critical value of ± 30 mV. Given the measured Z-potential values for the colloids (freshly and 120-days old samples, **Table S3**), they can be considered highly stable in agreement with the TEM results.

Table S3. Zeta-potential values for freshly and 120-days old MDR-EC-, EC-, MRSA-, SA-SeNPs

| Nanostructures | Z-potential (mV) | |
|----------------|------------------|-----------------|
| | As-synthesized | 120 days old |
| MDR-EC-SeNPs | -65 ± 10 | -60 ± 5 |
| EC-SeNPs | -73 ± 3 | -72 ± 2 |
| MRSA-SeNPs | -70 ± 3 | -67.3 ± 1.1 |
| SA-SeNPs | -67 ± 4 | -65 ± 5 |

The SeNPs were unlikely to form aggregates because of their electrostatic stability. Neutral and negatively charged NPs tend to have long half-lives in human serum and are not taken up by cells in a non-specific manner. This is important in the context of potential *in vivo* applications as antimicrobial reagents. Surface-associated bio(macro)molecules of the SeNPs capping layers were reported to be responsible for negative values of Z-potentials

owing to the presence of negatively charged functional groups (e.g., ionized carboxyl moieties)^{14,15}. These similarly charged groups serve as an additional factor stabilizing SeNPs in aqueous suspensions and their morphology during their biogenesis.

S.9. SEM observation of antimicrobial activity of the SeNPs on bacterial cells

For the fixation of bacterial cells, the different bacterial strains were inoculated into 4 mL of sterile LB media in a 15 mL Falcon conical centrifuge tube and incubated at 37 °C/200 rpm for 24 h. The optical density was then measured at 600 nm (OD₆₀₀) using a spectrophotometer. The overnight suspension was diluted to a final bacterial concentration of 10⁶ colony-forming units per milliliter (CFU/mL) before measuring the optical density. A selected 75 µg/mL concentration of MRSA-SeNPs, MDR-EC-SeNPs, SA-SeNPs, and EC-SeNPs was mixed with LB media and bacterial solution in a 6-well plate with a glass coverslip attached to the bottom. The coverslips were pre-treated with poly-lysine to enhance cell adhesion just before the experiment. The plate was placed inside an incubator for 8 h at 37 °C. After the experiments, the coverslips were fixed with a primary fixative solution containing 2.5% glutaraldehyde and 0.1 M sodium cacodylate buffer solution for 1 hour. Subsequently, the fixative solution was exchanged for 0.1 M sodium cacodylate buffer, and the coverslips were washed 3 times for 10 min. Post-fixation was done using 1% osmium tetroxide (OsO₄) solution in the buffer for 1 h. Subsequently, the coverslips were washed three times with buffer, and dehydration was progressively achieved with 30, 50, 70, 80, 95, and 100% ethanol (three times for the 100% ethanol). Finally, the coverslips were dried by liquid CO₂-ethanol exchange in a Samdri®-PVT-3D Critical Point Dryer. The coverslips were mounted on SEM stubs with carbon adhesive tabs (Electron Microscopy Sciences, EMS) after treatment with liquid graphite and then sputter-coated with a thin layer of platinum using a Cressington 208HR High-Resolution Sputter Coater. Digital images of the treated and untreated bacteria were acquired using a SEM.

For simplicity, only MDR-EC and MRSA experiments are shown where both bacteria were used as targets for the SeNPs. SEM micrographs of the control MDR-EC and MRSA (**Figures S18A** and **S18C**, respectively) and bacteria after treatment with MDR-EC-SeNPs and MRSA-SeNPs (**Figures S18B** and **S18D**, respectively) were taken to analyze further the effect of the SeNPs within the bacterial media.

The images indicated that the treatment with the bacteriogenic Se structures induced a change of both bacterial strains. Disruption of the outer cell membrane and cell lysis were observed after the treatment. Therefore, apparent cell damage was induced, quantified by a variable number of holes, cracks, and structural disruptions of the membranes. Furthermore, deformation and collapse of the bacterial structure were also found in some samples. The overproduction of ROS due to the presence of the SeNPs in the media is often a trigger of damages in the bacterial membranes. Nevertheless, other mechanisms can also be inferred, like those related to metal ion release or the impact of morphological features of the NPs themselves. From the SEM images of the bacteria, it is possible to see that membrane damage occurred as well as the attachment of nanoparticles to bacteria.

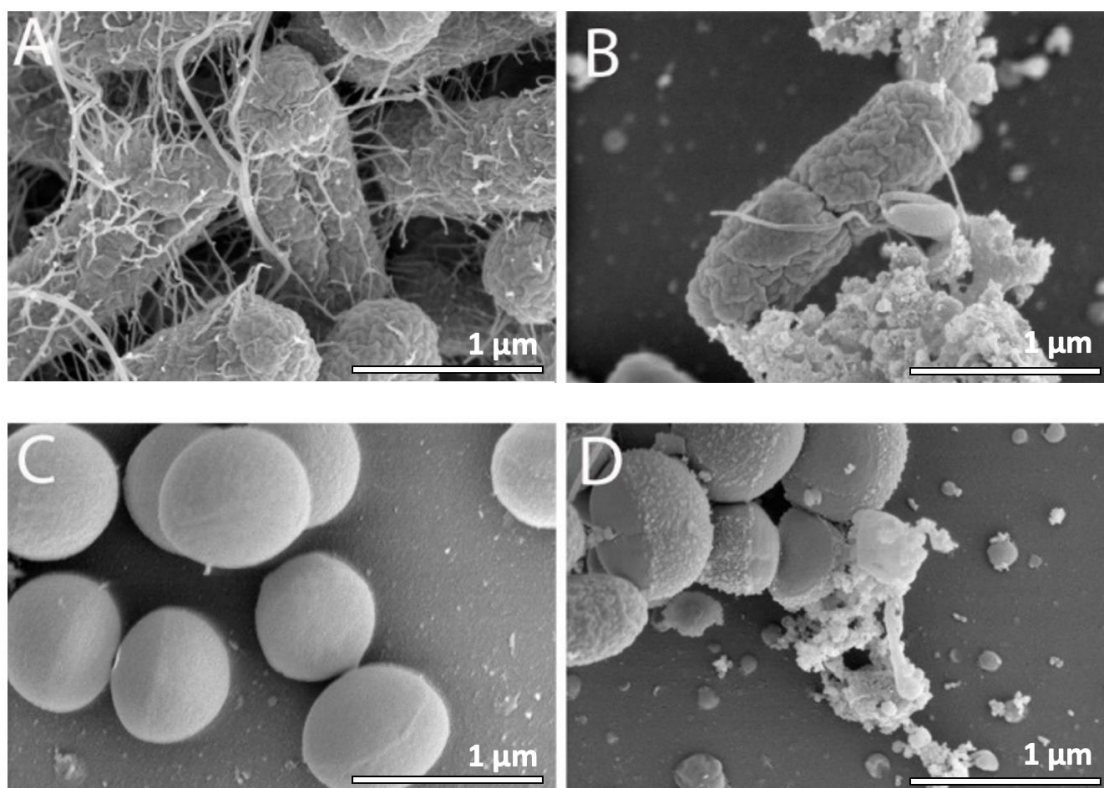


Figure S18. SEM micrographs of the control MDR-EC and MRSA (A, C) and bacteria post-treatment with MDR-EC-SeNPs and MRSA-SeNPs (B, D), respectively.

S.10. Antimicrobial tests for indirect experiments

The indirect analysis for EC (Figures S19A and S19B) and MDR-EC (Figures S19C and S19D) treated with different SA- and MRSA-SeNPs showed no inhibition at all. Therefore, it was possible to conclude that there is no significant antimicrobial effect when the SeNPs made by SA or MRSA target different bacterial species.

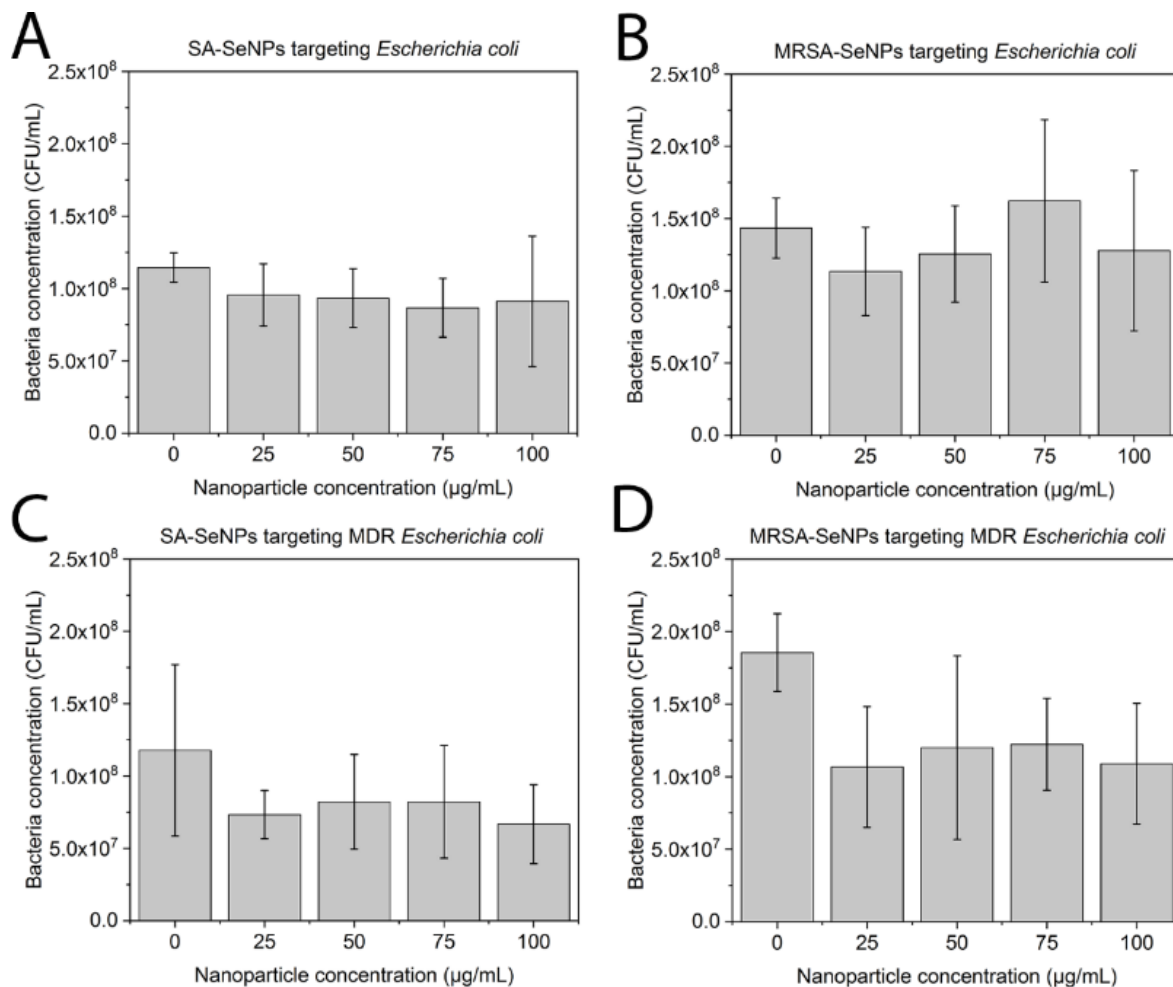


Figure S19. Colony counting assay of EC (A, B) and MDR-EC (C, D) after 8 h exposure to different SeNPs. Data is represented by the mean \pm Standard error of the mean. $N = 3$. Statistical differences represented by $*p < 0.05$ versus control, $**p < 0.01$ versus control.

The indirect analysis for *Staphylococcus aureus* (Figures S20A and S20B) and MRSA (Figures S20C and S20D) treated with different EC- and MDR-EC-SeNPs showed no inhibition at all. Therefore, it was possible to conclude that there was no significant antimicrobial effect when the NPs made by EC or MDR-EC targeted different bacterial species.

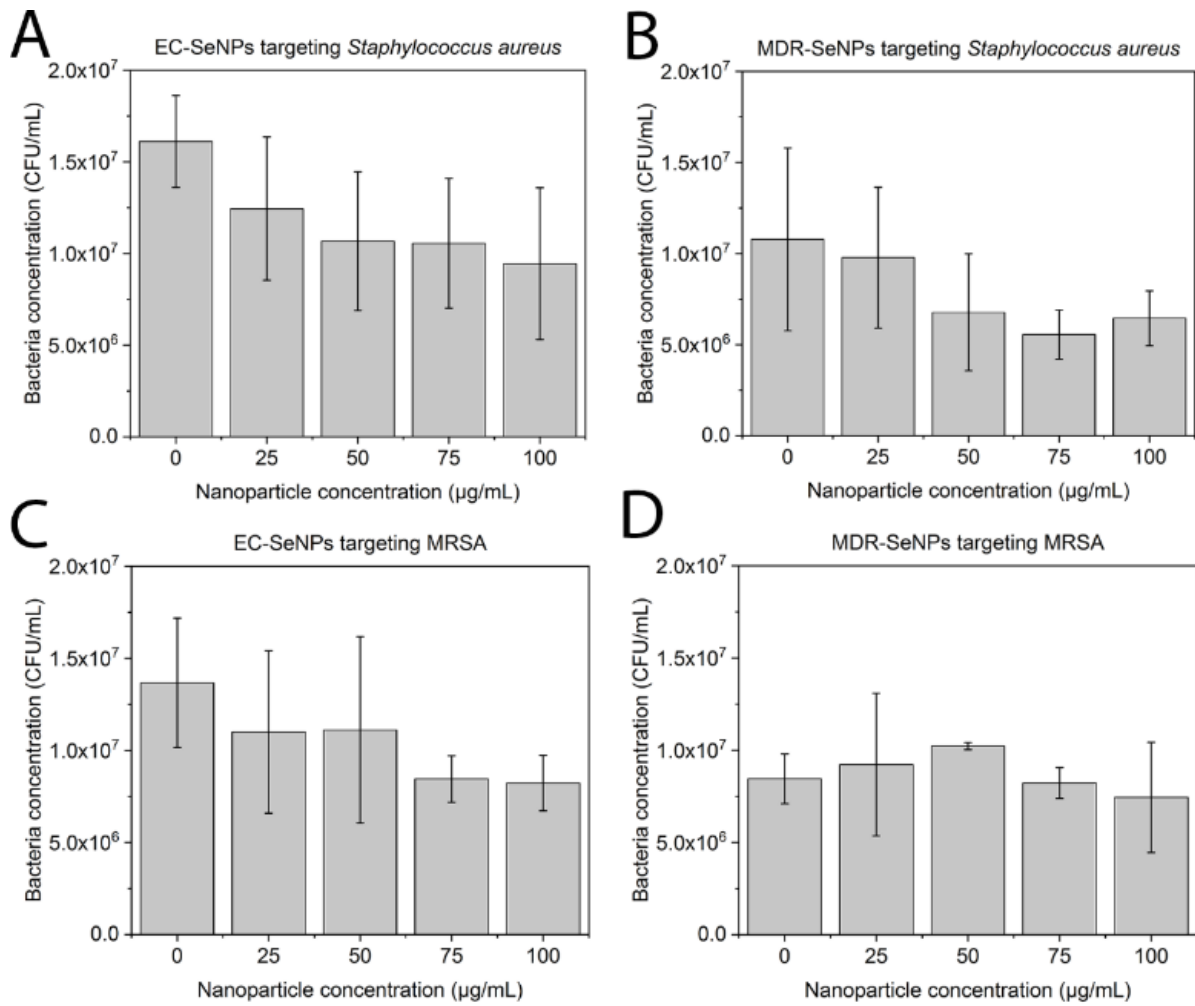


Figure S20. Colony counting assay of SA (A, B) and MRSA (C, D) after 8 h exposure to different SeNPs. Data is represented by the mean \pm Standard error of the mean. $N = 3$. Statistical differences represented by * $p < 0.05$ versus control, ** $p < 0.01$ versus control.

References

- (1) Mogensen, K. B.; Kneipp, K. Size-Dependent Shifts of Plasmon Resonance in Silver Nanoparticle Films Using Controlled Dissolution: Monitoring the Onset of Surface Screening Effects. *J. Phys. Chem. C* **2014**, *118* (48), 28075–28083. <https://doi.org/10.1021/jp505632n>.
- (2) Peng, S.; McMahon, J. M.; Schatz, G. C.; Gray, S. K.; Sun, Y. Reversing the Size-Dependence of Surface Plasmon Resonances. *Proc. Natl. Acad. Sci. U. S. A.* **2010**, *107* (33), 14530–14534. <https://doi.org/10.1073/pnas.1007524107>.
- (3) Kumar, A.; Bera, S.; Singh, M.; Mondal, D. Agrobacterium-Assisted Selenium Nanoparticles: Molecular Aspect of Antifungal Activity. *Adv. Nat. Sci. Nanosci. Nanotechnol.* **2017**, *9* (1), 015004. <https://doi.org/10.1088/2043-6254/aa9f4a>.
- (4) Vahdati, M.; Tohidi Moghadam, T. Synthesis and Characterization of Selenium Nanoparticles-Lysozyme Nanohybrid System with Synergistic Antibacterial Properties. *Sci. Rep.* **2020**, *10* (1), 1–10. <https://doi.org/10.1038/s41598-019-57333-7>.
- (5) Alam, H.; Khatoon, N.; Khan, M. A.; Husain, S. A.; Saravanan, M.; Sardar, M. Synthesis of Selenium Nanoparticles Using Probiotic Bacteria *Lactobacillus Acidophilus* and Their Enhanced Antimicrobial Activity Against Resistant Bacteria. *J. Clust. Sci.* **2019**, 1–9. <https://doi.org/10.1007/s10876-019-01705-6>.
- (6) Birben, E.; Sahiner, U. M.; Sackesen, C.; Erzurum, S.; Kalayci, O. Oxidative Stress and Antioxidant Defense. *World Allergy Organization Journal*. BioMed Central Ltd. 2012, pp 9–19. <https://doi.org/10.1097/WOX.0b013e3182439613>.
- (7) Piacenza, E.; Presentato, A.; Bardelli, M.; Lampis, S.; Vallini, G.; Turner, R. J. Influence of Bacterial Physiology on Processing of Selenite, Biogenesis of Nanomaterials and Their Thermodynamic Stability. *Molecules* **2019**, *24* (14). <https://doi.org/10.3390/molecules24142532>.
- (8) Turner, R. J.; Weiner, J. H.; Taylor, D. E. Selenium Metabolism in *Escherichia Coli*. *BioMetals* **1998**, *11* (3), 223–227. <https://doi.org/10.1023/A:1009290213301>.
- (9) Lemmon, E. W.; McLinden, M. O.; Friend, and D. G. *NIST Chemistry WebBook, NIST Standard Reference Database*; 2017. <https://doi.org/10.18434/T4D303>.
- (10) Hantsche, H. High Resolution XPS of Organic Polymers, the Scienta ESCA300 Database. By G. Beamson and D. Briggs, Wiley, Chichester 1992, 295 Pp., Hardcover, £ 65.00, ISBN 0-471-93592-1. *Adv. Mater.* **1993**, *5* (10), 778–778. <https://doi.org/10.1002/adma.19930051035>.
- (11) Clark, D. T.; Feast, W. J.; Tweedale, P. J.; Thomas, H. R. ESCA Applied to Polymers. XXVI. Investigation of a Series of Aliphatic, Aromatic, and Fluorine-Containing Polycarbonates. *J. Polym. Sci. Polym. Chem. Ed.* **1980**, *18* (6), 1651–1664. <https://doi.org/10.1002/pol.1980.170180601>.

- (12) Beamson, G.; Briggs, D. High Resolution XPS of Organic Polymers: The Scienta ESCA300 Database (Beamson, G.; Briggs, D.). *J. Chem. Educ.* **1993**, *70* (1), A25. <https://doi.org/10.1021/ed070pa25.5>.
- (13) Miyamoto, Y. Structure and Phase Transformation of Rhombohedral Selenium Composed of Se₆ Molecules. *Jpn. J. Appl. Phys.* **1980**, *19*, 1813. <https://doi.org/10.1143/JJAP.19.1813>
- (14) Jain, R.; Jordan, N.; Weiss, S.; Foerstendorf, H.; Heim, K.; Kacker, R.; Hübner, R.; Kramer, H.; van Hullebusch, E. D.; Farges, F.; et al. Extracellular Polymeric Substances Govern the Surface Charge of Biogenic Elemental Selenium Nanoparticles. *Environ. Sci. Technol.* **2015**, *49* (3), 1713–1720. <https://doi.org/10.1021/es5043063>.
- (15) Kamnev, A. A.; Mamchenkova, P. V.; Dyatlova, Y. A.; Tugarova, A. V. FTIR Spectroscopic Studies of Selenite Reduction by Cells of the Rhizobacterium *Azospirillum Brasilense* Sp7 and the Formation of Selenium Nanoparticles. *J. Mol. Struct.* **2017**, *1140*, 106–112. <https://doi.org/10.1016/J.MOLSTRUC.2016.12.003>.